Supplementary Information

Npl4 decodes polyubiquitin length and gates D1-D2 coupling in human VCP/p97

Laxmikanta Khamari[1,4], Jingxuan Tang[1,4], Stephanie L. Moon[2,3], and Nils G. Walter[1,2]

[1]Department of Chemistry, University of Michigan, Ann Arbor, MI 48109, USA. [2]Center for RNA Biomedicine, University of Michigan, Ann Arbor, MI, USA. [3]Department of Human Genetics, University of Michigan, Ann Arbor, MI 48109, USA. [4]These authors contributed equally: Laxmikanta Khamari, Jingxuan Tang. ⊠e-mail: nwalter@umich.edu, smslmoon@umich.edu

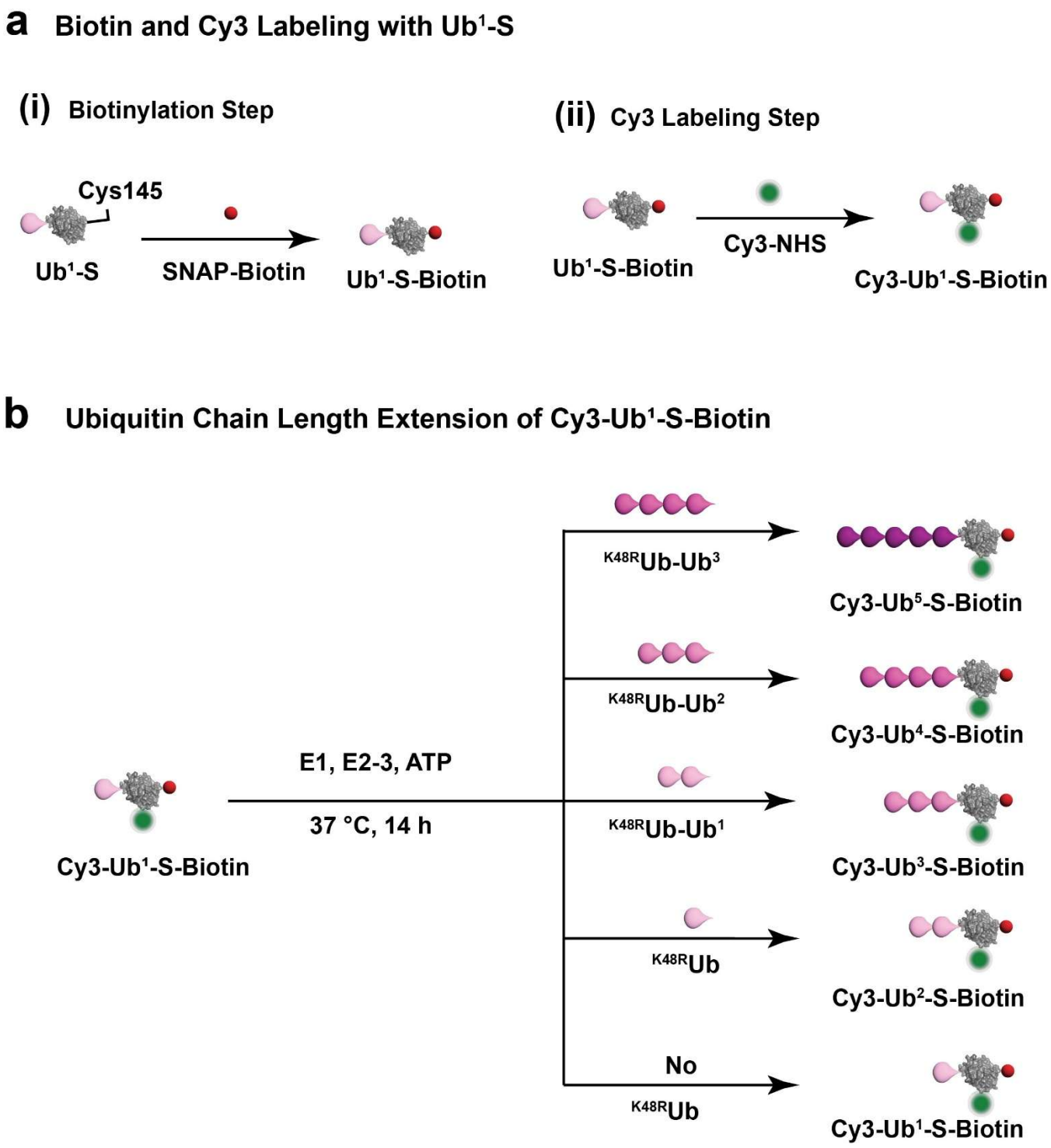

Supplementary Fig. 1| Stepwise biotinylation, fluorescent labelling, and polyubiquitination workflow. a Schematic overview of the sequential modification of Ub1-S, including (i) biotinylation for coverslip immobilization and (ii) Cy3 labeling for fluorescence imaging. **b** Workflow of the enzymatic polyubiquitination reaction used to generate ubiquitin substrates (here, SNAP-tag) of defined chain lengths for subsequent assays. Related to Figures 1 and 2.

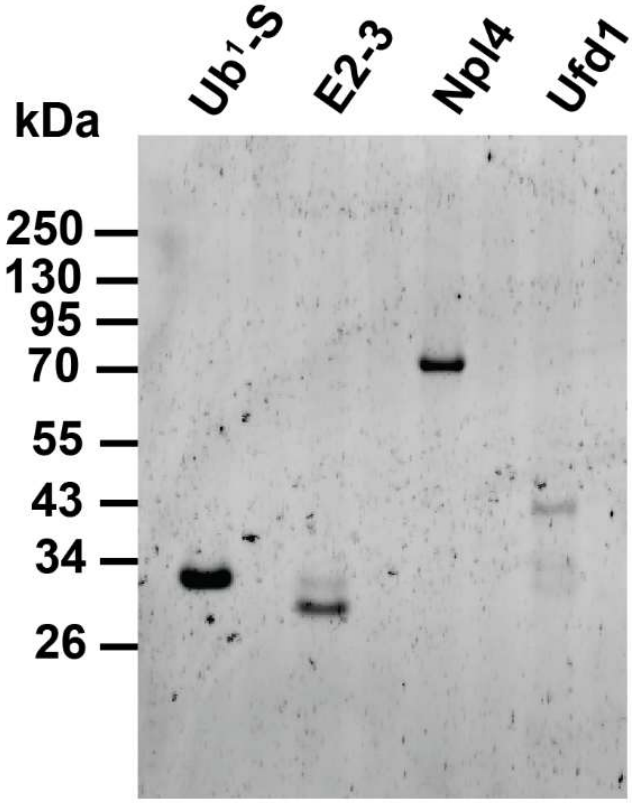

Supplementary Fig. 2| SDS-PAGE analysis of Ub^1-S, E2-3, Npl4, and Ufd1 used in this study.

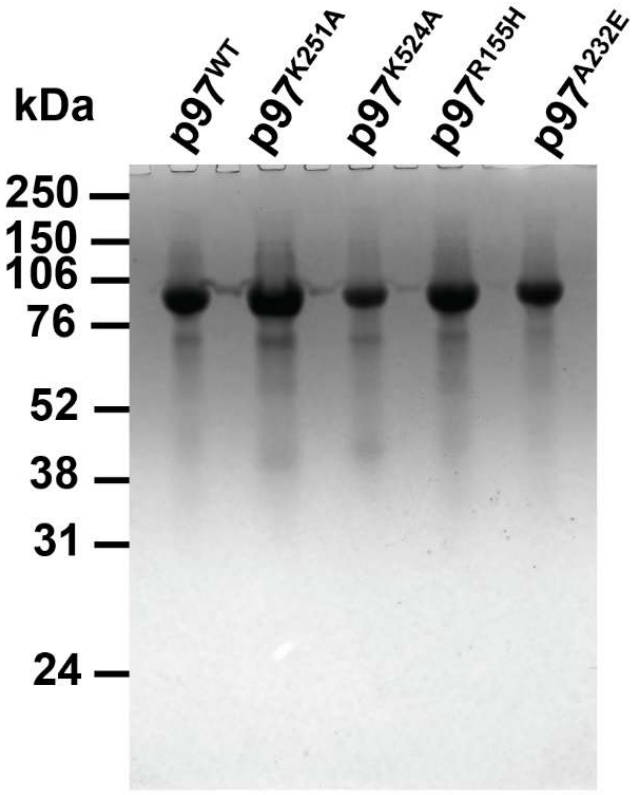

Supplementary Fig. 3| SDS-PAGE analysis of p97 variants used in this study.

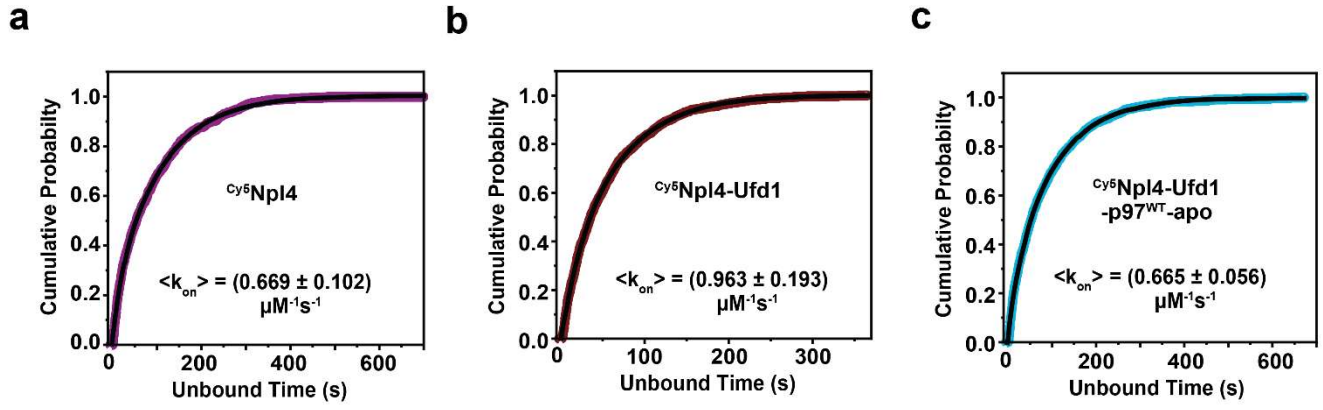

Supplementary Fig. 4| Binding kinetics of Npl4 to Ub^5-S and modulation by Ufd1 and p97. a–c Cumulative distributions of unbound dwell times for Cy5-labeled Npl4 interacting with Ub^5-S substrates under different conditions: (**a**) Npl4 alone, (**b**) in the formation of heterodimer with Ufd1, and (**c**) in association with the Ufd1–p97^{WT} complex. Related to Figure 3

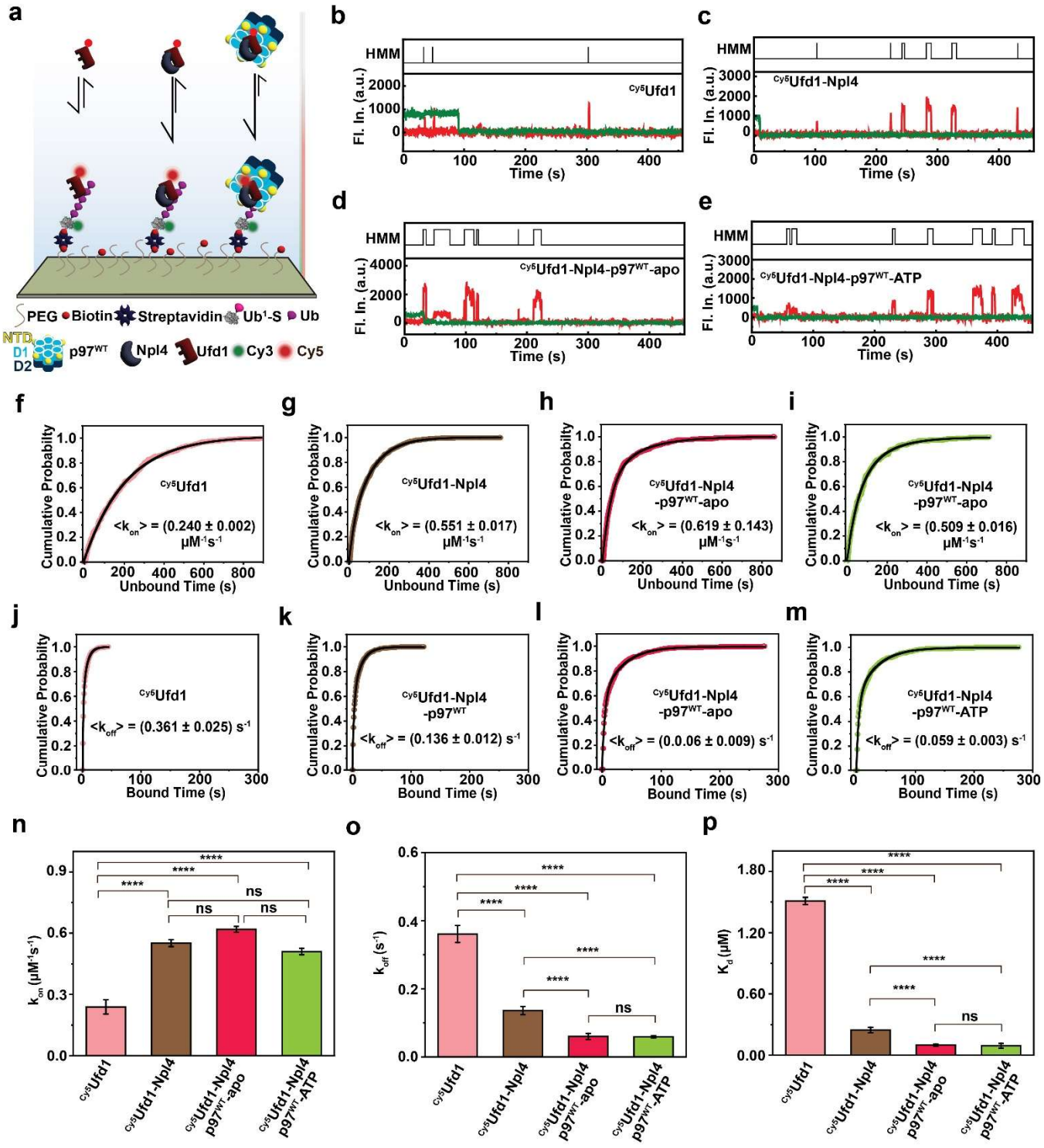

Supplementary Fig. 5| Binding dynamics of Ufd1 to Ub^5-S substrate in the presence of Npl4 and p97^{WT}. a Schematic representation of the experimental workflow used to measure association and dissociation kinetics of Cy5-labelled Ufd1 (^{Cy5}Ufd1) interacting with Ub^5-S substrates under three conditions: Ufd1 alone, Ufd1 following Npl4 heterodimer formation, and the Npl4–p97^{WT} complex. **b–e** Representative single-molecule fluorescence intensity time traces for ^{Cy5}Ufd1 binding to Ub^5-S under four

conditions: Ufd1 alone (**b**), following assembly with Npl4 (**c**), association with the Npl4–p97^{WT} complex in the absence of ATP (**d**), and after ATP addition (**e**). Segmentation via HMM analysis is indicated above each trace. **f–i** Cumulative distributions of unbound dwell times for ^{Cy5}Ufd1 on Ub^{5}-S, contrasting conditions with or without Npl4 and the Npl4–p97^{WT} complex, as shown. **j–m** Cumulative distributions of bound dwell times for ^{Cy5}Ufd1 on Ub^{5}-S, similarly comparing the relevant conditions, as discussed earlier. **n–p** Quantification of kinetic parameters: association rate constant (k_{on}), dissociation rate constant (k_{off}), and equilibrium dissociation constant (K_d) for ^{Cy5}Ufd1 binding to Ub^{5}-S under each condition. Statistical significance was determined using a two-tailed Student's t-test (ns, not significant; $0.05 < p \leq 0.5$; *$0.01 < p \leq 0.05$; **$0.001 < p \leq 0.01$; ***$0.0001 < p \leq 0.001$; ****$p \leq 0.0001$).

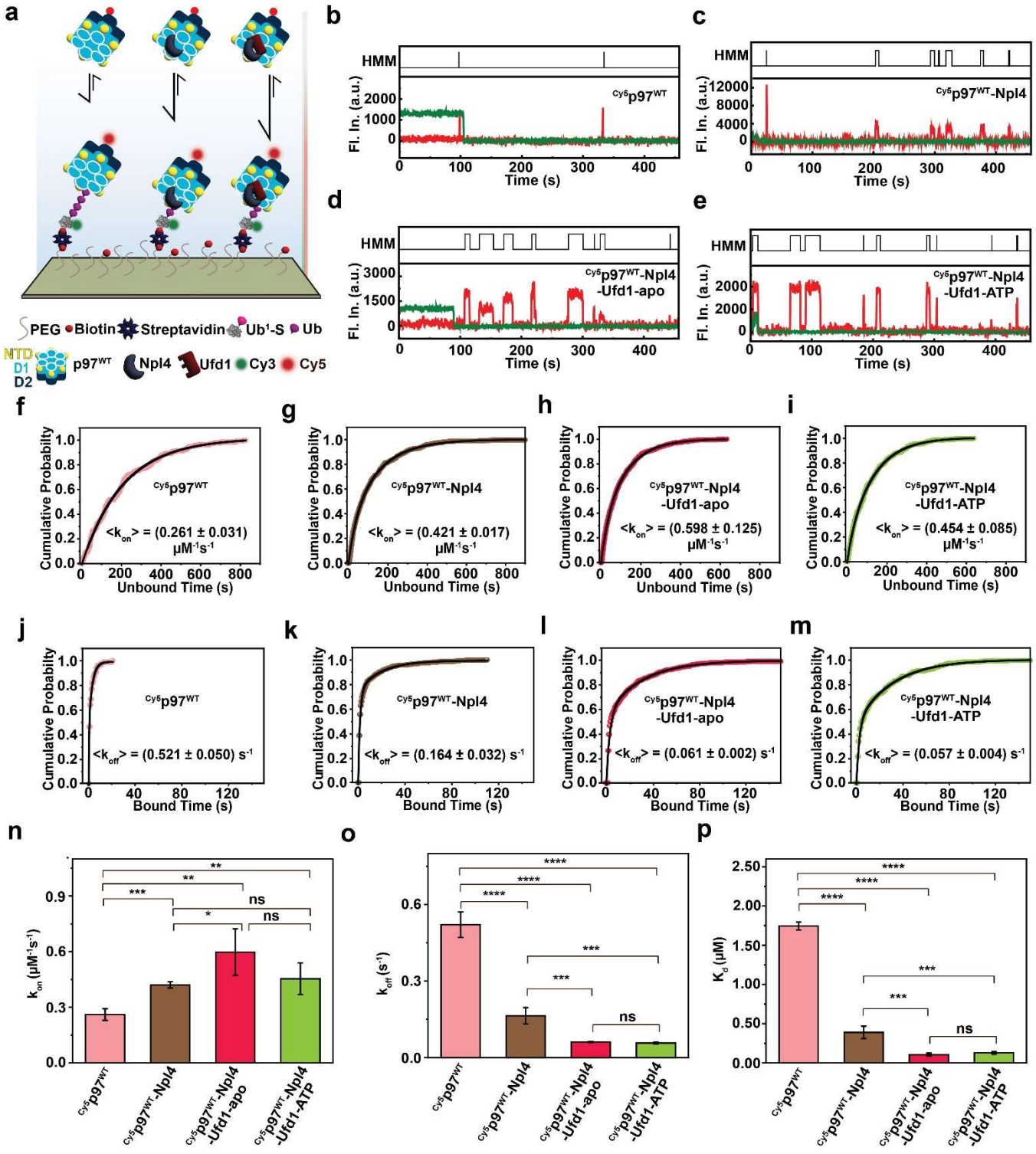

Supplementary Fig. 6| Binding dynamics of p97^{WT} to Ub^5-S substrate in the presence of Npl4 and Ufd1. a Diagram outlining the experimental setup used to monitor association and dissociation kinetics of Cy5-labelled p97^{WT} (^{Cy5}p97) binding to Ub^5-S substrates across three conditions: p97 alone, after incorporation with Npl4, and following assembly with the Npl4–Ufd1 complex. **b–e** Representative

single-molecule fluorescence intensity trajectories for ^{Cy5}p97 binding to Ub^5-S under four scenarios: p97 alone (**b**), after addition of Npl4 (**c**), association with the Npl4–Ufd1 complex under apo conditions (**d**), and upon ATP addition (**e**). HMM-based segmentations are shown above each trace. **f–i** Cumulative distribution curves of unbound dwell times for ^{Cy5}p97 interacting with Ub^5-S, comparing the presence and absence of Npl4 and the Npl4–Ufd1 complex. **j–m** Cumulative distributions of bound dwell times for ^{Cy5}p97 on Ub^5-S, comparing the specified conditions. **n–p** Quantitative analysis of kinetic parameters including association rate constant (k_{on}), dissociation rate constant (k_{off}), and equilibrium dissociation constant (K_d) for ^{Cy5}p97 binding to Ub^5-S in each experimental condition. Statistical significance was determined using a two-tailed Student's t-test (ns, not significant; $0.05 < p \leq 0.5$; *$0.01 < p \leq 0.05$; **$0.001 < p \leq 0.01$; ***$0.0001 < p \leq 0.001$; ****$p \leq 0.0001$).

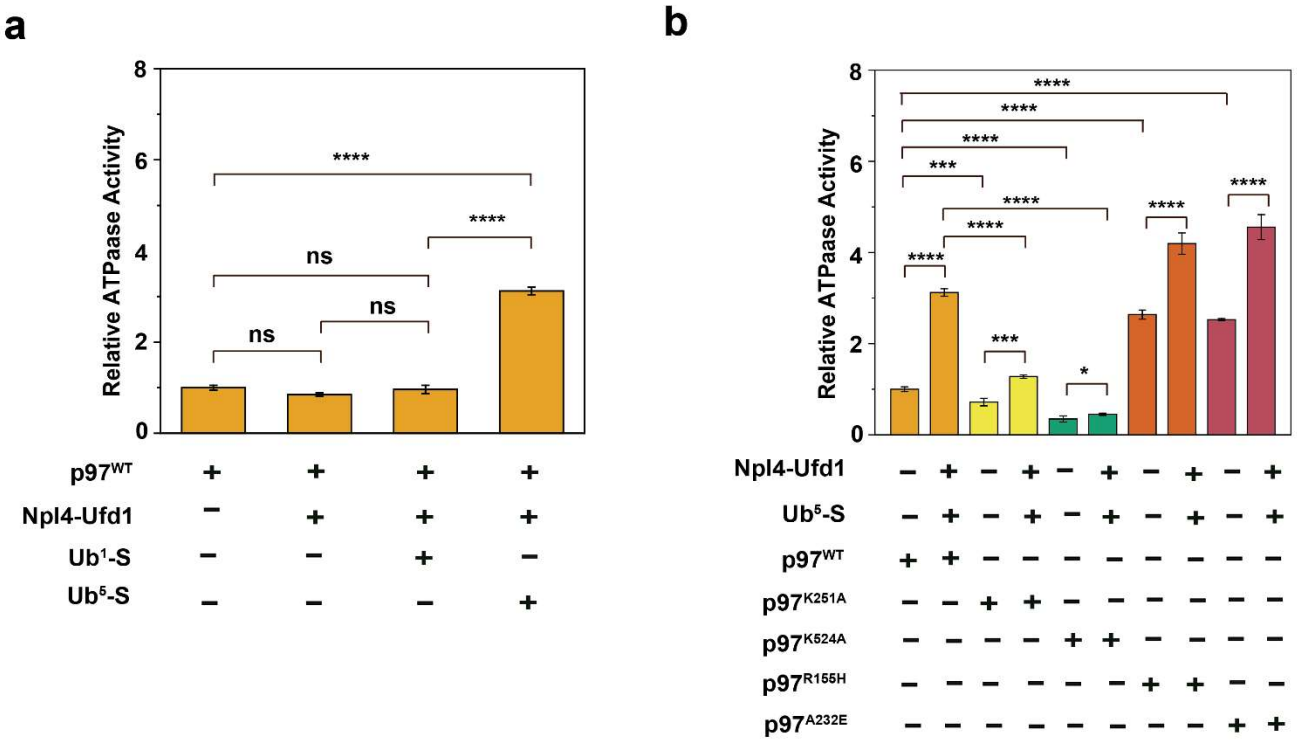

Supplementary Fig. 7| Substrate-dependent stimulation of p97 ATPase activity in presence of UN complex. a Relative ATPase activity of $p97^{WT}$ was assessed under various conditions: with or without the Npl4-Ufd1 cofactors, and in the presence of different ubiquitin substrates. While, Ub^1-S and UN alone did not affect p97 ATPase activity, the addition of penta-ubiquitin (Ub^5-S) resulted in a threefold increase. **b** Comparison of ATPase activity across p97 variants (WT, K251A, K524A, R155H, and A232E) with or without Npl4-Ufd1 and Ub^5-S. Measurements were performed using BIOMOL Green and normalized to basal $p97^{WT}$ activity. The D1 mutant, K251A showed a 29% reduction, and the D2 mutant K524A a 65% reduction in basal activity compared to WT. Addition of Npl4-Ufd1 and Ub^5-S led to a slight recovery in ATPase activity for these mutants. Pathogenic variants R155H and A232E exhibited elevated basal ATPase activity—4 fold and 4.5-fold above WT, respectively—consistent with previous reports. Furthermore, ATPase activity in these mutants increased significantly with the introduction of cofactors and substrate, surpassing that observed in WT and in substrate-free conditions. Data are presented as mean ± SD (n = 3). Statistical significance was determined using a two-tailed Student's t-test (ns, not significant; $0.05 < p \leq 0.5$; *$0.01 < p \leq 0.05$; **$0.001 < p \leq 0.01$; ***$0.0001 < p \leq 0.001$; ****$p \leq 0.0001$).

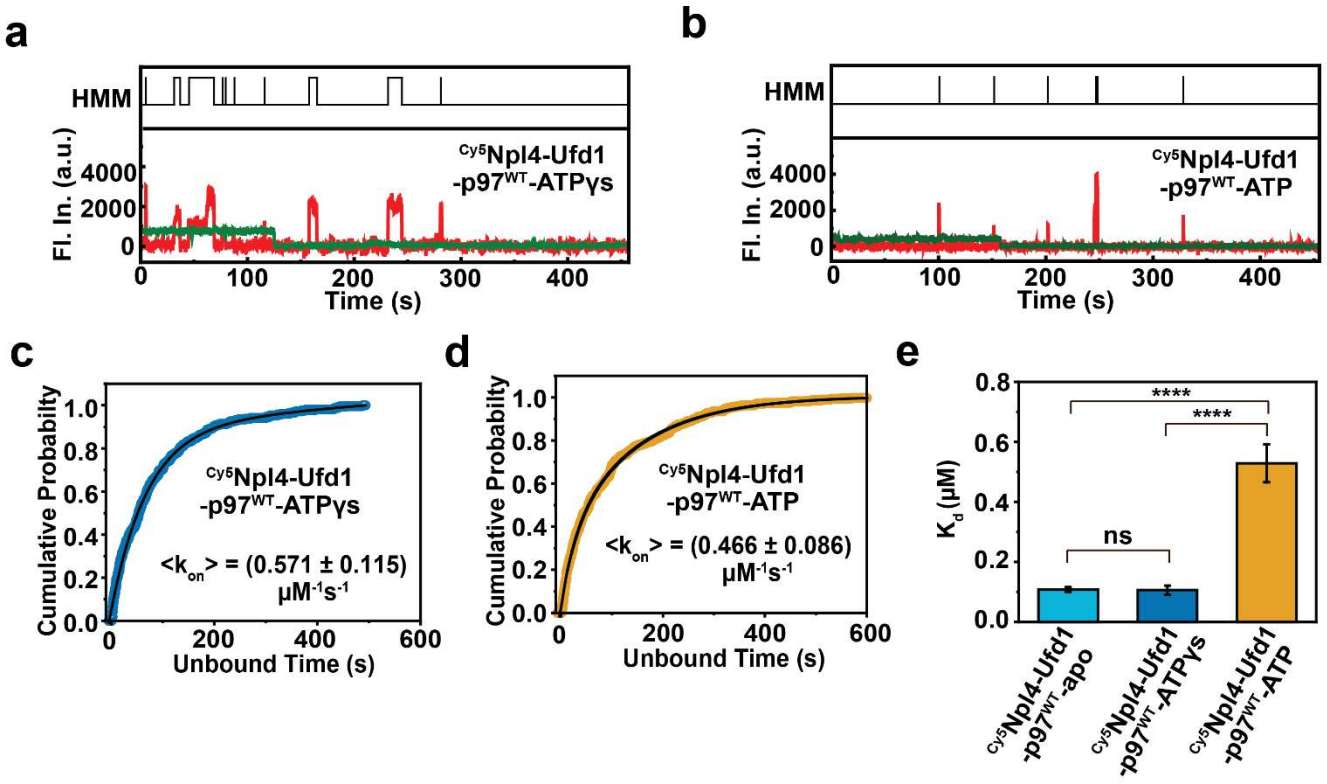

Supplementary Fig. 8| Dynamic exchange of Npl4 within the Npl4–Ufd1–p97^{WT}–Ub^{5}-S complex is modulated by p97 conformational changes under distinct nucleotide states. a-b Representative single-molecule fluorescence intensity trajectories for Cy5-labelled Npl4 (^{Cy5}Npl4) (preassembled with Npl4–Ufd1–p97^{WT}) bound to Ub^{5}-S substrate, under ATPγS (**a**) and ATP (**b**) conditions, illustrating nucleotide-dependent alterations in Npl4 binding dynamics. HMM-derived segmentations are displayed above each trace. **c–d** Cumulative distributions of unbound dwell times for ^{Cy5}Npl4 (preassembled with Npl4–Ufd1–p97^{WT}) on Ub^{5}-S substrate under ATPγS (**c**) and ATP (**d**) conditions, highlighting unaltered in association rate constants related to nucleotide state. **e** Quntifiaction of equilibrium dissociation constant (K_d) for ^{Cy5}Npl4 binding to Ub^{5}-S across the two nucleotide states. Statistical significance was evaluated by two-tailed Student's t-test (ns, not significant; $0.05 < p \leq 0.5$; *$0.01 < p \leq 0.05$; **$0.001 < p \leq 0.01$; ***$0.0001 < p \leq 0.001$; ****$p \leq 0.0001$). Related to Figure 4.

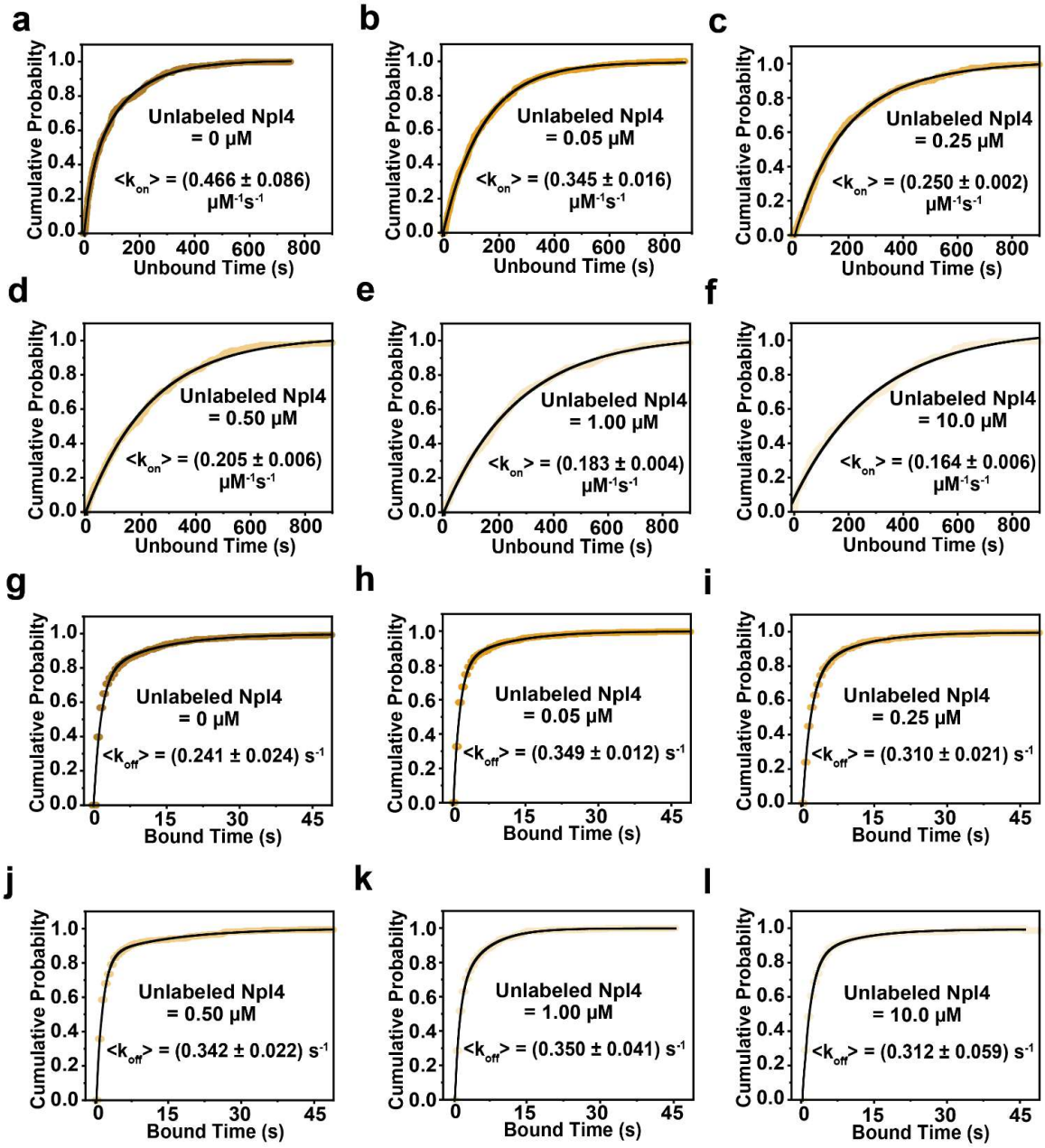

Supplementary Fig. 9| Conformational changes in p97 during ATP hydrolysis modulate dynamic Npl4 exchange within the Npl4–Ufd1–p97^{WT}–Ub^{5}-S complex. a–f Cumulative distributions of unbound dwell times for Cy5-labeled Npl4 (^{Cy5}Npl4), preassembled with the Npl4–Ufd1–p97^{WT} complex, on Ub^{5}-S substrate under ATP hydrolysis conditions, with increasing concentrations of unlabeled Npl4 ([unlabeled Npl4] = 0, 0.05, 0.25, 0.50, 1.0, and 10.0 μM; ^{Cy5}Npl4 = 20 nM). The data indicate a stepwise increase in association rate constants as the concentration of unlabeled Npl4 rises, reflecting enhanced Npl4 exchange within the complex during p97 ATP hydrolysis. **g–i** Cumulative distributions of bound dwell times for ^{Cy5}Npl4 (preassembled with Npl4–Ufd1–p97^{WT}) bound to Ub^{5}-S substrate under identical ATP hydrolysis conditions and increasing concentrations of unlabeled Npl4, demonstrate that dissociation rate constants remain largely unchanged, regardless of added unlabeled Npl4. Figure 4 for related data.

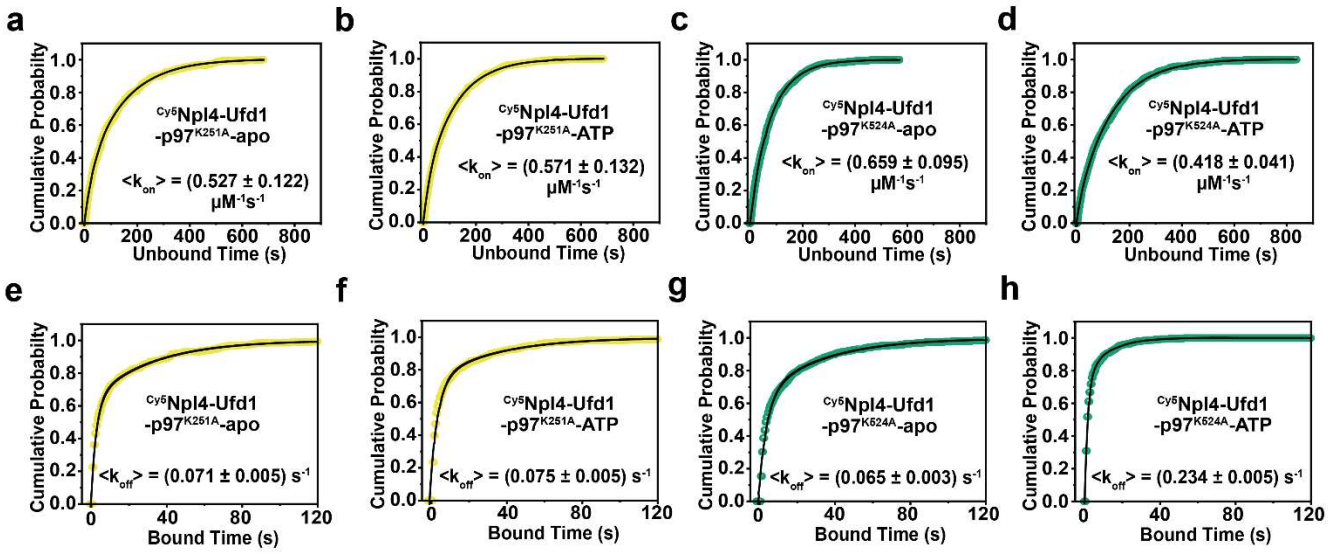

Supplementary Fig. 10| D1-specific ATP hydrolysis facilitates dynamic Npl4 exchange on substrate. **a-b** Cumulative distributions of unbound dwell times for ^{Cy5}Npl4, preassembled with the Npl4–Ufd1–p97^{K251A} complex (D1 domain inactive, D2 domain active), interacting with Ub^5-S substrate in the absence (**a**) and presence (**b**) of ATP. **c-d** Cumulative distributions of unbound dwell times for ^{Cy5}Npl4 preassembled with the Npl4–Ufd1–p97^{K524A} complex (D1 domain active, D2 domain inactive) on Ub^5-S substrate, without ATP (**c**) and after ATP addition (**d**). **e-f** Cumulative distributions of bound dwell times for ^{Cy5}Npl4 with the Npl4–Ufd1–p97^{K251A} complex on Ub^5-S, comparing conditions without (**e**) and with (**f**) ATP. **g-h** Cumulative distributions of bound dwell times for ^{Cy5}Npl4 with the Npl4–Ufd1–p97^{K524A} complex on Ub^5-S substrate, without (**g**) and with (**h**) ATP. See Figure 4 for related results.

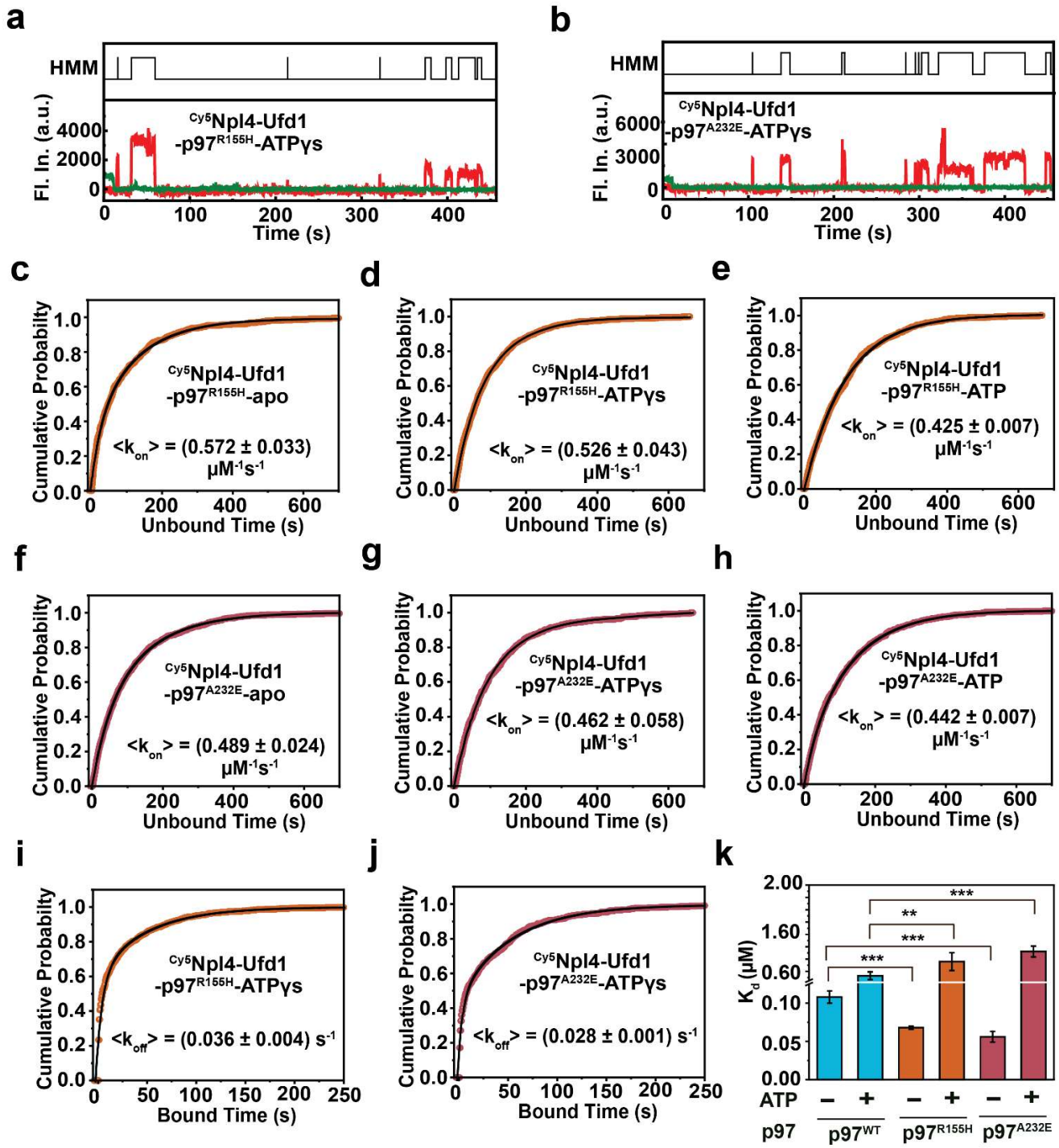

Supplementary Fig. 11| Disease-associated p97 mutants R155H and A232E enhance substrate affinity and disrupt Npl4–Ufd1–p97 complex dynamics. a-b Representative single-molecule fluorescence intensity trajectories for ^{Cy5}Npl4, preassembled with Npl4–Ufd1–p97, binding to Ub^5-S substrate under ATPγS conditions for the R155H (**a**) and A232E (**b**) p97 variants. HMM-segmented regions are indicated above each trace. **c–e** Cumulative distributions of unbound dwell times for ^{Cy5}Npl4 (assembled with Npl4–Ufd1–p97^{R155H}) binding to Ub^5-S substrate in the nucleotide-free, apo (**c**), ATPγS

(**d**), and ATP (**e**) conditions, showing minimal changes in association rate constants across nucleotide states. **f–h** Cumulative distributions of bound dwell times for ^{Cy5}Npl4 (with Npl4–Ufd1–p97^{A232E}) on Ub^{5}-S substrate under apo (**f**), ATPγS (**g**), and ATP (**h**) conditions, indicating similar association kinetics regardless of nucleotide state. **i** Quantification of equilibrium dissociation constant (K_d) for ^{Cy5}Npl4 binding to Ub^{5}-S across apo and nucleotide conditions for p97^{WT} and the pathogenic mutants p97^{R155H} and p97^{A232E}. Statistical significance determined using two-tailed Student's t-test (ns, not significant; $0.05 < p \leq 0.5$; *$0.01 < p \leq 0.05$; **$0.001 < p \leq 0.01$; ***$0.0001 < p \leq 0.001$; ****$p \leq 0.0001$). See Figure 5 for related data.

Table S1: Proteins used in this study

Plasmid name	Vector	Antibiotic Resistance	Expression	Purification	Comments	Source
Ub[1]-SNAP-tag-6xHis	pET-28a	KAN	BL21 (DE3), 0.6 mM IPTG, TB, 18 °C for 14 h	Ni-NTA, His-Trap column	-	This study
6xHis-TEV-gp78-Ube2g2	pET-28a	KAN	BL21 (DE3), 0.4 mM IPTG, TB, 25 °C for 16 h	Ni-NTA, TEV cleavage, His-Trap column	-	*Proc. Natl Acad. Sci. USA* **114**, E4380–E4388 (2017) Ref[2]
Npl4	pET41b+	AMP	BL21 (DE3), 0.4 mM IPTG, TB, 18 °C for 14 h	Ni-NTA, His-Trap column	Co-express and co-purified with Ufd1-8XHis	Addgene
6xHis-TEV-Npl4	pET-28a	KAN	BL21 (DE3), 0.4 mM IPTG, TB, 18 °C for 14 h	Ni-NTA, TEV cleavage, His-Trap column	-	This study
Ufd1-8XHis	pET41b+	KAN	BL21 (DE3), 0.4 mM IPTG, TB, 18 °C for 14 h	Ni-NTA, His-Trap column	-	Addgene
6xHis-TEV-Ufd1	pET-28a	KAN	BL21 (DE3), 0.4 mM IPTG, TB, 18 °C for 14 h	Ni-NTA, TEV cleavage, His-Trap column	-	This Study
$p97^{WT}$-HA-6xHis	pET-28a	KAN	BL21 (DE3), 1 mM IPTG, TB, 25 °C for 12 h	Ni-NTA, His-Trap column	-	This study

$p97^{K251A}$-HA-6xHis	pET-28a	KAN	BL21 (DE3), 1 mM IPTG, TB, 25 °C for 12 h	Ni-NTA, His-Trap column	-	This study
$p97^{K524A}$-HA-6xHis	pET-28a	KAN	BL21 (DE3), 1 mM IPTG, TB, 25 °C for 12 h	Ni-NTA, His-Trap column	-	This study
$p97^{R155H}$-HA-6xHis	pET-28a	KAN	BL21 (DE3), 1 mM IPTG, TB, 25 °C for 12 h	Ni-NTA, His-Trap column	-	This study
$p97^{A232E}$-HA-6xHis	pET-28a	KAN	BL21 (DE3), 1 mM IPTG, TB, 25 °C for 12 h	Ni-NTA, His-Trap column	-	This study

Table S2: Commercial proteins and chemicals used in this study

Protein name	Catalog Number#	Source
UBE1	UB-0101-005	LifeSensors
Ub	U-100H	Bio-Techne
$^{K48R}Ub^{1}$	SI217	LifeSensors
^{K48R}Ub-Ub^{1}	SI4802	LifeSensors
^{K48R}Ub-Ub^{2}	SI4803	LifeSensors
^{K48R}Ub-Ub^{3}	SI4804	LifeSensors
Cyanine3 NHS ester	11020	Lumiprobe
Cyanine5 NHS ester	13020	Lumiprobe